GCY-8, PDE-2, and NCS-1 are critical elements of the cGMP-dependent thermotransduction cascade in the AFD neurons responsible for *C. elegans* thermotaxis

Dong Wang,[1] Damien O'Halloran,[2,3] and Miriam B. Goodman[1]

[1]Department of Molecular and Cellular Physiology, Stanford University School of Medicine, Stanford, CA 94305
[2]Department of Biological Sciences and [3]Institute for Neuroscience, George Washington University, Washington, DC 20052

Certain thermoreceptor neurons are sensitive to tiny thermal fluctuations (0.01°C or less) and maintain their sensitivity across a wide range of ambient temperatures through a process of adaptation, but understanding of the biochemical basis for this performance is rudimentary. Prior studies of the AFD thermoreceptor in *Caenorhabditis elegans* revealed a signaling cascade that depends on a trio of receptor guanylate cyclases (rGCs), GCY-8, GCY-18, and GCY-23, and gives rise to warming-activated thermoreceptor currents (ThRCs) carried by cyclic GMP–gated ion channels. The threshold for ThRC activation adapts to the ambient temperature through an unknown calcium-dependent process. Here, we use in vivo whole-cell patch-clamp recording from AFD to show that loss of GCY-8, but not of GCY-18 or GCY-23, reduces or eliminates ThRCs, identifying this rGC as a crucial signaling element. To learn more about thermotransduction and adaptation, we used behavioral screens and analysis of gene expression patterns to identify phosphodiesterases (PDEs) likely to contribute to thermotransduction. Deleting PDE-2 decouples the threshold for ThRC activation from ambient temperature, altering adaptation. We provide evidence that the conserved neuronal calcium sensor 1 protein also regulates the threshold for ThRC activation and propose a signaling network to account for ThRC activation and adaptation. Because PDEs play essential roles in diverse biological processes, including vertebrate phototransduction and olfaction, and regulation of smooth muscle contractility and cardiovascular function, this study has broad implications for understanding how extraordinary sensitivity and dynamic range is achieved in cyclic nucleotide–based signaling networks.

The Journal of General Physiology

INTRODUCTION

Animals have evolved specialized thermoreceptor neurons to monitor and detect changes in ambient and internal temperature. In nematodes (Hedgecock and Russell, 1975; Ryu and Samuel, 2002; Luo et al., 2006) and certain beetles (Schmitz and Trenner, 2003; Must et al., 2010), snakes (Gracheva et al., 2010), and bats (Campbell et al., 2002; Gracheva et al., 2011), a temperature change of 0.01°C or less is sufficient to activate such neurons through a process of sensory thermotransduction. Such extraordinary sensitivity is reflected in apparent Q_{10} values that approach 10^{20} in pit vipers (Bullock and Diecke, 1956) and nematodes (Ramot et al., 2008a). Thus, extraordinary temperature sensitivity is conserved in diverse animals. As in photoreceptors, high sensitivity is maintained over a wide dynamic range through adaptation to constant ambient temperatures. But understanding of the molecular and cellular machinery responsible for converting minute thermal fluctuations into biologically relevant neural signals remains rudimentary.

Caenorhabditis elegans nematodes exhibit defined behavioral responses to spatial thermal gradients that are straightforward to measure in the laboratory, a feature that makes these animals an excellent model for probing the mechanism of thermotransduction (Ryu and Samuel, 2002). In the common laboratory strain of *C. elegans* (N2), thermal gradients evoke two distinct behaviors. The first is negative thermotaxis or migration toward cooler temperatures. This is the dominant behavior whenever the ambient temperature exceeds the growth or cultivation temperature, T_c, and is achieved by means of a biased random walk (Hedgecock and Russell, 1975; Mori and Ohshima, 1995; Ryu and Samuel, 2002; Ramot et al., 2008b). The second behavior, isothermal tracking, is observed when animals reach thermal zones that are within 2°C of T_c (Hedgecock and Russell, 1975; Ryu and Samuel, 2002; Biron et al., 2006; Chi et al., 2007). Simple assays that examine migration in thermal gradients have been exploited to uncover many of the genes and cells required for thermosensation (Mori and Ohshima, 1995; Mori, 1999; Garrity et al., 2010).

Correspondence to Miriam B. Goodman: mbgoodman@stanford.edu
D. Wang's present address is Dept. of Anesthesiology, Stanford University School of Medicine, Palo Alto, CA 94304.

Abbreviations used in this paper: GCAP, guanylate cyclase–activating protein; IBMX, 3-isobutyl-1-methylxanthine; NCS-1, neuronal calcium sensor 1; PDE, phosphodiesterase; rGC, receptor guanylate cyclase; ThRC, thermoreceptor current.

The Rockefeller University Press $30.00
J. Gen. Physiol. Vol. 142 No. 4 437–449
www.jgp.org/cgi/doi/10.1085/jgp.201310959

These behaviors involve at least three pairs of bipolar thermoreceptor neurons: AFD, AWC, and ASI neurons (Mori and Ohshima, 1995; Biron et al., 2008; Kuhara et al., 2008; Beverly et al., 2011). This study concerns the AFD neurons, whose sensory dendrites terminate in a specialized ending comprised of a primary cilium and an extensive array of microvilli (Ward et al., 1975; White et al., 1986). At least five genes are known to be essential for thermotransduction by AFD (Garrity et al., 2010): *tax-4* and *tax-2*, which encode the α and β subunits of a CNG ion channel, and *gcy-8*, *gcy-18*, and *gcy-23*, which encode receptor guanylate cyclases (rGCs) and are exclusive to the AFD neurons. Warming-evoked thermoreceptor currents (ThRCs) in AFD are carried by a nonselective cation channel that depends on *tax-4* and *tax-2* (Ramot et al., 2008a). Such currents exhibit the extraordinary sensitivity (apparent Q_{10} values exceed 10^{15}) required for a single neuron to detect temperature changes of 0.01°C or less and are eliminated in *gcy-8–gcy-18–gcy-23* triple mutants. We argued previously that the large values for apparent Q_{10} are an emergent property of nonlinear amplification in the thermotransduction network in AFD rather than a reflection of the temperature dependence of any one element in this network (Ramot et al., 2008a). By analogy to the well-established mechanism for phototransduction in vertebrate rods and cones (Fu and Yau, 2007; Fain et al., 2010; Arshavsky and Burns, 2012), we previously hypothesized that thermotransduction in AFD neurons involves temperature-dependent regulation of the concentration of cGMP (Ramot et al., 2008a).

In this study, we investigate the cyclic nucleotide phosphodiesterase (PDE), whose contribution to AFD thermotransduction has not been addressed previously. There are six *pde* genes in the *C. elegans* genome: *pde-1*, *pde-2*, *pde-3*, *pde-4*, *pde-5*, and *pde-6*. Based on the study of human PDE proteins (Omori and Kotera, 2007), it was proposed that PDE-4 and PDE-6 proteins are cAMP-specific PDEs, and the other four PDEs can cleave both cAMP and cGMP. At present, our knowledge of PDE-mediated signaling in *C. elegans* is limited. Nevertheless, it has been reported that PDE-1 and PDE-5 are involved in the G protein–mediated, cGMP-dependent regulation of adult lifespan extension (Hahm et al., 2009), whereas PDE-1, PDE-2, PDE-3, and PDE-5 all contribute to phototransduction in *C. elegans* UV photoreceptors (Liu et al., 2010).

Combining behavioral studies and in vivo whole-cell patch-clamp recording, we show that thermotaxis behavior depends on a suite of PDEs and identify *pde-2* as an essential element of the thermotransduction cascade in AFD. Specifically, we found that mutating the *pde-2* gene prolongs ThRCs and elevates their threshold for activation. With the same approaches, we show that loss of GCY-8 eliminates ThRCs in AFD. We additionally address the contribution of neuronal calcium sensor 1 (NCS-1), a calcium-binding protein related to vertebrate guanylate cyclase–activating proteins (GCAPs) and 74% identical to human frequenin (Shaye and Greenwald, 2011), to membrane current in AFD. As found for *pde-2* mutants, loss of NCS-1 prolongs ThRCs and elevates their threshold. However, unlike loss of PDE-2, which has no effect on voltage-activated currents, loss of NCS-1 increases voltage-activated outward currents. This work implies that a signaling network incorporating GCY-8, PDE-2, and NCS-1 proteins regulates ThRCs by controlling intracellular cGMP levels in a temperature-dependent manner.

MATERIALS AND METHODS

Strains and chemicals

The following strains were used in this work: GN2 *oyIs17*(Pgcy-8::GFP), GN112 *pgIs2*(Pgcy-8::Caspase), *gcy-8(oy44)gcy-23(nj37)* IV, *gcy-8(oy44)gcy-18(nj38)* IV, IK597 *gcy-8(oy44)* IV *gcy-18(nj38)* IV *gcy-23(nj37)*, FX03765 *pde-1(tm3765)* I, FX03098 *pde-2(tm3098)* III, FX01998 *pde-3(tm1998)* II, FX03617 *pde-5(tm3617)* I, N2(wild-type) Bristol, PY5664 *gcy-8(oy44)* IV; *oyIs17*, PY5665 *gcy-18(nj38)* IV; *oyIs17*, PY5666 *gcy-23(nj37)* IV; *oyIs17*, PY7502 (recCaspase under the control of AWC-specific P*ceh*-36; P*srtx-1*::AWC), PY7504 (recCaspase under the control of P*gpa*-4 and P*gcy-27*; P*gcy-27*::GFP), TQ1828 *pde-1(nj57) pde-5(nj49)* I; *pde-3(nj59)* II; *pde-2(tm3098)* III, XA406 *ncs-1(qa406)* X. These researchers provided strains of the following: I. Mori (Nagoya University, Nagoya, Japan) provided IK strains and the *gcy-8(oy44)gcy-23(nj37)* and *gcy-8(oy44)gcy-18(nj38)* double mutants; S. Mitani and the National BioResource Project of Japan provided FX strains; P. Sengupta (Brandeis University, Waltham, MA) provided PY strains; and S. Xu (University of Michigan, Ann Arbor, MI) provided TQ strains.

We generated mutant animals that expressed GFP in AFD neurons by crossing *oyIs17* into FX03098 *pde-2(tm3098)*, FX03617 *pde-5(tm3617)*, and XA406 *ncs-1(qa406)* X, resulting in the following strains: GN454 *pde-2(tm3098)* III; *oyIs17*, GN455 *pde-5(tm3617)* I; *oyIs17*, GN474 *pde-5(tm3617)* I; *pde-2(tm3098)* III; *oyIs17* and GN476 *ncs-1(qa406)* X; and *oyIs17*. For all experiments, we used age-synchronized L4 larvae or young adult animals. Animals were synchronized using standard methods (Fay, 2006).

The PDE-2–selective inhibitor BAY-60-7550 was purchased from Cayman Chemical. All chemicals were purchased from Sigma-Aldrich.

Thermal migration assay

Wild-type and mutant animals were tested for their ability to migrate toward cooler temperatures in linear thermal gradients of 0.5, 1.0, and 1.5°C/cm, as described previously (Ramot et al., 2008b; Glauser et al., 2011). In brief, we transferred ∼100–400 well-fed young adult worms to the center of assay plates and allowed them to migrate for 10 min. For all assays, the starting temperature (T_s) was 3°C higher than the cultivation temperature (T_c). Prior studies showed that wild-type animals exhibit robust negative thermotaxis under these conditions (Ramot et al., 2008b). At the end of the 10-min assay period, we took a digital photograph of each assay plate and used particle-tracking tools in ImageJ to determine animal position. From these data, we compute the thermotaxis index, TI = (W − C)/(W + C), where W and C are the total number of worms on the warmer and cooler sides of the assay plate, respectively.

Promoter GFP fusions for *pde* genes

Promoter GFP fusions were generated as described previously (Hobert, 2002). Primers designed to the upstream of the predicted start codon of *pde-1* (4,765 bp upstream of T04D3.3a), *pde-2* (4,721 bp upstream of R08D7.6a), *pde-3* (3,030 bp upstream of

E01F3.1b), and *pde-5* (2,035 bp upstream of C32E12.2) were used to PCR amplify predicted promoter sequences (Hi-Fidelity polymerase; Roche). We used PCR to fuse these amplicons to a GFP product that included the *unc-54* 3′UTR, amplified from the plasmid pPD95.75 (available from AddGene: http://www.addgene.org/1494/) with these primers: GFP-F: AGCTTGCATGCCTGCAGGTCGACT and GFP-R: AAGGGCCCGTACGGCCGACTAGTAGG.

Fusion PCR was performed using 10 ng of each amplicon with a nested promoter-specific primer and the GFP-nested primer: GGAAACAGTTATGTTTGGTATATTGGG. Fusion products were purified and injected into wild-type (N2) animals at ∼100 ng/µl. To mark the AFD neuron, we built a coinjection marker by cloning a fragment of the *gcy-8* promoter sequence into a modified pPD95.75 vector in which the coding sequence for mCherry replaced the coding sequence for GFP. Primers used to amplify the *gcy-8* promoter sequence were: gcy8-F: ggccggCTGCAGgtgacatgcgatcaagaattttggttcaacaagg and gcy8-R: ggccggGGTACCcgaaaatcctttacagcttctcacgatagttacc.

These primers contained the restriction sites for PstI and KpnI to facilitate cloning the promoter element into the pPD95.75 plasmid. This coinjection marker was injected with the fusion products at 30 ng/µl. Stable transgenic lines were imaged using a confocal system (LSM 510; Carl Zeiss) at a magnification of 63.

In vivo electrophysiology

Recordings were obtained essentially as described previously (Ramot et al., 2008a), with the following modifications. In brief, we immobilized animals using special-purpose cyanoacrylate glue (WormGlu; GluStitch Inc.) on a thin layer of 2% agarose in a coverslip (No. 1; VWR International) and exposed the GFP-labeled AFD soma by opening a tiny slit in the cuticle with a sharpened glass probe. Animals were active at least for 1 h when provided with a continuous flow of fresh external saline.

We fabricated recording pipettes from borosilicate glass capillaries (outside diameter, 1.5 mm; inside diameter, 0.86 mm; BF15086-10; Sutter Instrument) and used pressure polishing (Goodman and Lockery, 2000; Johnson et al., 2008; Goodman et al., 2012) to achieve resistances of 6–12 MΩ when filled with the internal saline. 10 mM sulforhodamine-101 (Molecular Probes) was included in the pipette to monitor the appearance of the AFD neuron during and after the recording. Pipette capacitance and the liquid junction potential of +14 mV were compensated during recording with an EPC-10 amplifier and Patchmaster software (HEKA).

Recording solutions

Standard external saline contained (mM): 145 NaCl, 5 KCl, 5 $MgCl_2$, 1 $CaCl_2$, and 10 Na-HEPES, pH adjusted to 7.2 with NaOH. 20 mM glucose was added before each experiment to reach a final osmolarity of ∼325 mOsm. Pipettes were filled with internal saline containing (mM): 125 K-gluconate, 18 KCl, 4 NaCl, 1 $MgCl_2$, 0.6 $CaCl_2$, 10 K-HEPES, and 10 K_2EGTA, pH adjusted to 7.2 with KOH. To increase recording duration and minimize rundown of both ThRCs and voltage-activated outward currents, 5 mM Na_2ATP and 0.5 mM Na_2GTP were also included. 10 mM sulforhodamine-101 (Molecular Probes) was added to the pipette solution, which had an osmolarity of ∼315 mOsm.

Temperature- and voltage-activated currents

During in vivo recording, we used a thermoelectric heater/cooler (SC-20/CL-100; Warner Instruments) to deliver external saline at defined temperatures under computer control, as described previously (Ramot et al., 2008a). We continuously monitored the temperature achieved near each target animal by positioning a small, cylindrical thermistor (TA-29; Warner Instruments) nearby and used the EPC-10 to digitize this signal in parallel with membrane currents. All thermal stimuli consisted of ramps that cooled animals to ∼15°C, warmed them to ∼25°C, and returned to a defined holding temperature. Thermal ramps were generated at a rate of ∼0.2°C/s. Membrane currents induced by the thermal ramp were sampled at 1 kHz and filtered at 400 Hz.

Voltage-activated currents were measured from the response to a series of pulses between −110 and +100 mV (in 20-mV increments). As described by Ramot et al. (2008a), residual capacity currents were subtracted and average peak and steady-state currents were derived from the average of three presentations of the family of voltage pulses. Membrane current was sampled at 5 kHz and filtered at 2 kHz.

Data analysis

Electrophysiological data were acquired with PatchMaster and analyzed using Igor Pro 6.0 software (WaveMetrics). We determined input capacitance and series resistance as described previously (Goodman et al., 1998). Only recordings with a holding current less than −10 pA (at −60 mV) and a series resistance <180 MΩ were retained for further analysis. Series resistance was not compensated during recording because the voltage error for ThRCs is <3 mV (V_{hold} = −60 mV). Neither series resistance nor input capacitance varied as a function of genotype, and the average values were (mean ± SEM; n = 92) 130 ± 3 MΩ (range: 55–179 MΩ) and 1.51 ± 0.04 pF (range: 0.82 – 2.44 pF), respectively. We verified that recordings were obtained from AFD neurons with intact neurites by visual inspection of sulforhodamine-101 loading (included in the recording pipette). Pulses used to determine the capacitance and series resistance were sampled at 10 kHz and filtered at 2.9 kHz.

The amplitude of warming-activated ThRCs was determined with an automatic peak-finding function (Igor Pro 6.0), and their half-maximal duration was defined as the time elapsed between the half-maxima of the rising and falling phase of ThRCs. We estimated apparent Q_{10} values from Arrhenius plots derived by plotting the normalized current, $(I_m - I_0)/I_0$, as a function of inverse temperature (in degrees K), as described previously (Ramot et al., 2008a). Here, I_m is the current during thermal stimulation, and I_0 is the holding current before applying thermal stimulation. Values for apparent Q_{10} were derived from the activation energy (E_a) estimated from the slope of linear fit line in the Arrhenius plot: $-E_a = R \ln(I_2/I_1)/(1/T_2 - 1/T_1)$, where I_1 and I_2 are the normalized current amplitude at lower (T_1) and higher (T_2) temperatures, respectively, and R is the gas constant. The apparent Q_{10} is then given by $Q_{10} = \exp(10E_a/RT_1T_2)$. The threshold temperature (T^*) was obtained from the intersection of the linear fit to the two phases of ThRCs.

Statistics

All pooled, averaged data are expressed as mean ± SEM. Statistical analysis was performed with Student's t test in Origin 7.0 (OriginLab), and $P < 0.05$ was considered statistically significant.

Online supplemental material

Fig. S1 compares the response of wild-type animals with that of *gcy-8–gcy-18*, *gcy-18–gcy-23*, and *gcy-18–gcy-23* double mutants to shallow and steep linear thermal gradients. Fig. S2 compares the thermotaxis response of intact wild-type animals to that of transgenic animals lacking the AFD, AWC, and ASI sensory neurons. The online supplemental material is available at http://www.jgp.org/cgi/content/full/jgp.201310959/DC1.

RESULTS

GCY-8, but not GCY-18 and GCY-23, is required for negative thermotaxis

A trio of rGC genes, *gcy-8*, *gcy-18*, and *gcy-23*, are co-expressed only in the AFD neurons (Inada et al., 2006),

which play a critical role in isothermal tracking (Beverly et al., 2011; Wasserman et al., 2011) and migration in linear thermal gradients (Glauser et al., 2011). Animals with defects in all three genes fail to respond to thermal gradients (Inada et al., 2006; Beverly et al., 2011) and lack detectable ThRCs (Ramot et al., 2008a). Consistent with these prior studies, we found that *gcy-8–gcy-18–gcy-23* triple mutants have strong defects in negative thermotaxis, regardless of either cultivation temperature or gradient steepness (Fig. 1, A–C). Mutants lacking either *gcy-18* or *gcy-23* performed like wild-type animals under most conditions tested (Fig. 1, B and C). In contrast, *gcy-8* mutants cultivated at 15°C responded poorly to shallow gradients of 0.5°C/cm but behaved more like wild-type animals on steeper gradients (Fig. 1, A and B). The behavioral defect in *gcy-8* mutants was T_c dependent: mutants grown at 15°C fail to detect shallow gradients, whereas those grown at 20°C exhibit only a mild defect (Fig. 1 C). We reasoned that if *gcy-8* were the dominant rGC, then animals lacking *gcy-18* and *gcy-23* but retaining an intact *gcy-8* gene should have nearly wild-type performance. Consistent with this idea, the thermotaxis index of *gcy-18–gcy-23* double mutants was similar to wild type under most conditions (Fig. S1). Similarly, the behavior of *gcy-8–gcy-18* and *gcy-8–gcy-23* double mutants was similar to that of *gcy-8* single mutants (Fig. S1). Collectively and consistent with prior work (Inada et al., 2006; Wasserman et al., 2011), these behavioral studies suggest that neither *gcy-18* nor *gcy-23* can compensate for the loss of *gcy-8*, and that *gcy-8* plays a dominant and central role in AFD.

ThRCs require GCY-8, but not GCY-18 or GCY-23

Next, we used in vivo whole-cell patch-clamp recording to directly compare ThRCs in wild-type, *gcy-8*, *gcy-18*, and *gcy-23* single mutant AFD neurons. As we have shown previously (Ramot et al., 2008a), wild-type ThRCs activate upon warming to a threshold temperature, T^*, and exhibit an extraordinary temperature dependence, with current reaching its maximum value within 1°C of warming. ThRCs are carried by cations and depend on expression of TAX-4 and TAX-2 (Ramot et al., 2008a), subunits of a CNG ion channel. We found that ThRCs were absent in *gcy-8* mutant AFD neurons but were retained and indistinguishable from wild type in *gcy-18* and *gcy-23* mutant AFD neurons (Fig. 2, A and D). Loss of *gcy-8*, *gcy-18*, or *gcy-23* had no obvious effect on the amplitude or time course of voltage-activated membrane currents (Fig. 2, B and C), indicating that the effect of *gcy-8* loss of function was specific to ThRCs and that *gcy-18* and *gcy-23* make little, if any, contribution to ionic currents in AFD.

The lack of detectable ThRCs in *gcy-8* AFD neurons was unexpected, as *gcy-8* single mutants have minor defects in thermal migration (Fig. 1, B and C). The simplest interpretation of these findings is that other neurons

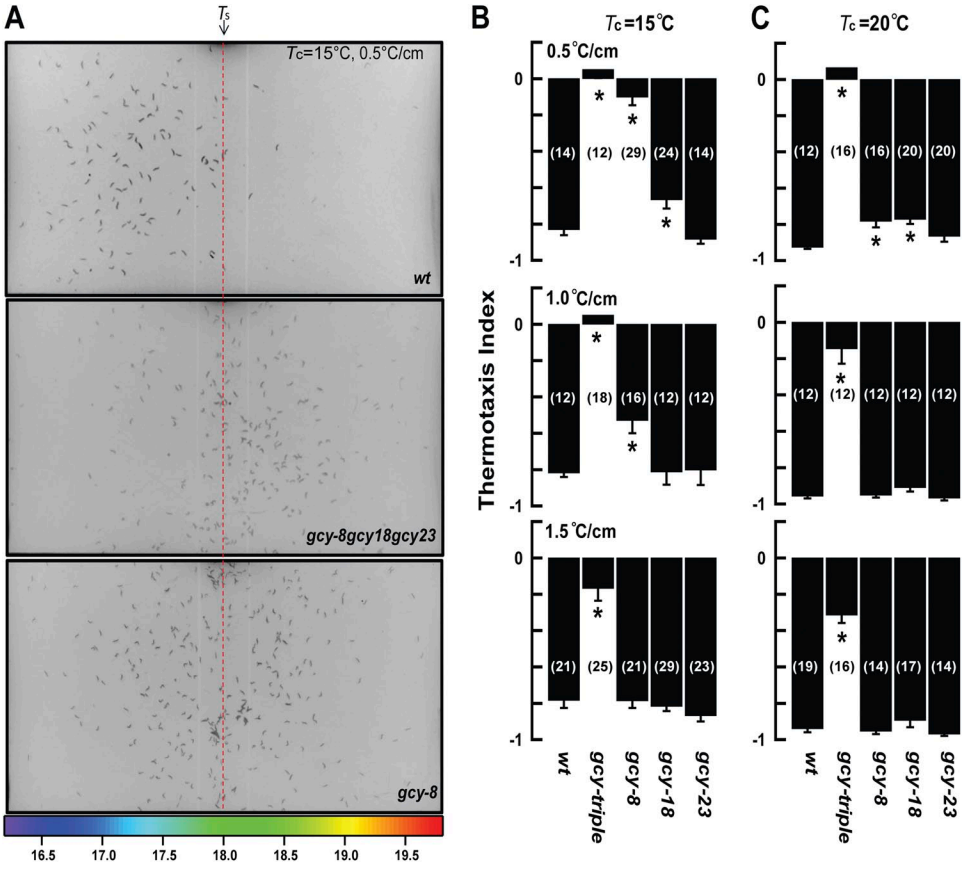

Figure 1. GCY-8 is required for proper thermotaxis. (A) Representative images of wild-type (*wt*), *gcy-8*, and *gcy-8–gcy-18–gcy-23* triple mutants after exposure to linear thermal gradients (0.5°C/cm). Worms appear as black marks in this digital image. The dashed line (red) indicates the starting temperature (T_s) of 18°C. All animals were cultivated at 15°C. (B and C) Thermotaxis response profiles of *gcy* mutants at T_c = 15°C and T_c = 20°C. Bars are mean ± SEM; the number of assays is indicated in parentheses. *, $P < 0.05$ compared with wild type.

partially compensate for the loss of AFD signaling in *gcy-8*. Evidence supporting this idea comes from experiments showing that AFD, AWC, and ASI all contribute to thermotaxis behavior (Fig. S2 and Beverly et al., 2011). These results imply that GCY-8 is an essential element of the thermotransduction cascade in AFD and that animals can partially compensate for the loss of GCY-8–dependent AFD signaling through the action of other thermoreceptor neurons.

PDE inhibitors increase *T** and induce longer-lived ThRCs

One working model for thermotransduction posits that temperature regulates the concentration of cGMP in the sensory ending (Inada et al., 2006), a process that could include temperature-dependent regulation of both the synthesis and hydrolysis of cGMP. PDEs are conserved enzymes that convert cyclic nucleotides to their monophosphate cognates and are inhibited non-specifically by 3-isobutyl-1-methylxanthine (IBMX). We used IBMX to determine whether or not PDE function was required for AFD thermotransduction, comparing ThRCs in the absence and presence of IBMX. Fig. 3 shows that although ThRCs were retained in the presence of IBMX, they were longer-lived and had a higher *T** than in the absence of the drug. This result suggests that one or more PDEs help to shape ThRCs in AFD.

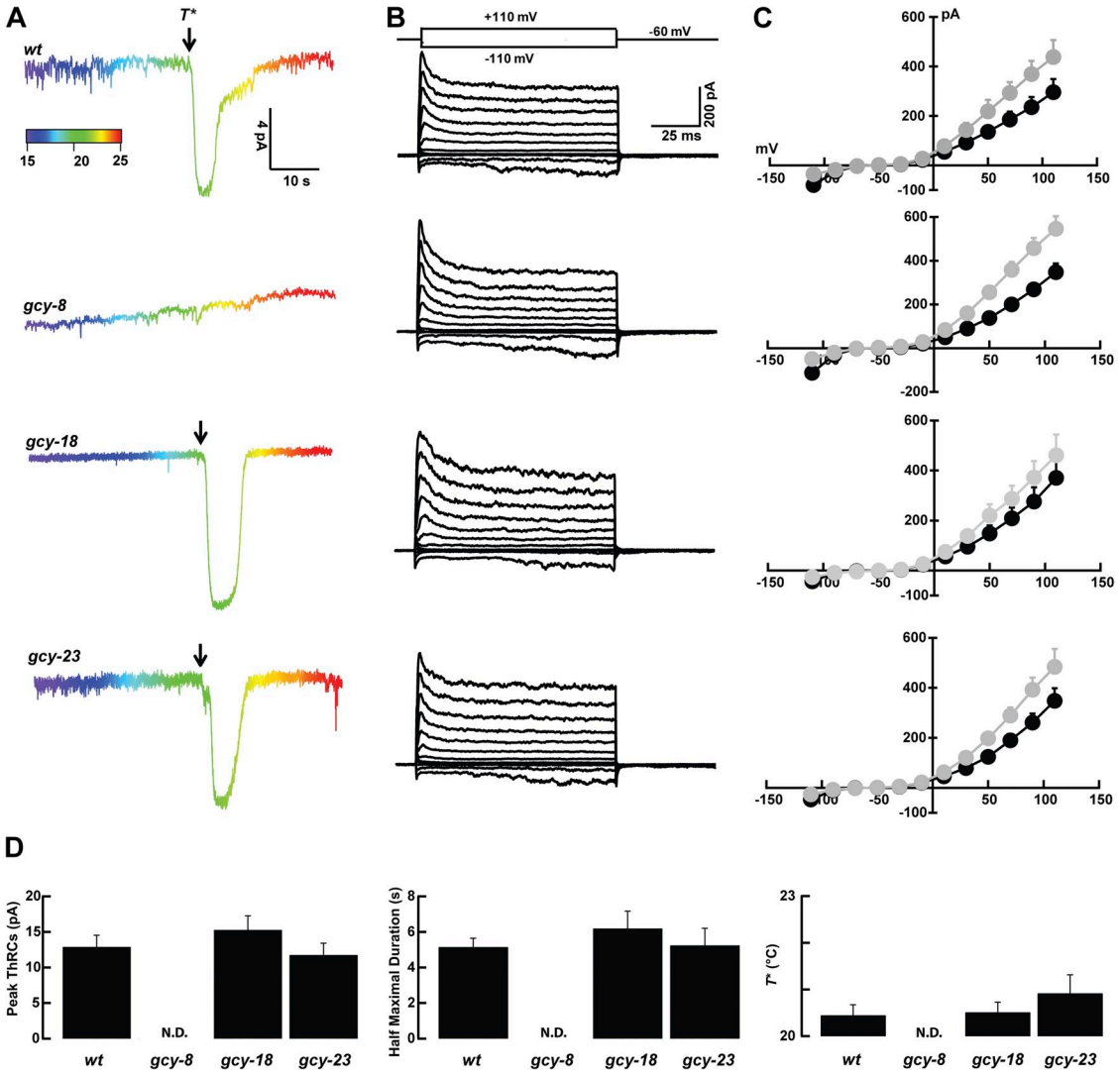

Figure 2. Loss of GCY-8, but not GCY-18 or GCY-23, eliminates AFD ThRCs. (A) Warming-evoked ThRCs from AFD neurons in (top to bottom): wild-type (*wt*), *gcy-8*, *gcy-18*, and *gcy-23* AFD neurons. V_{hold} = −60 mV. Arrows indicate *T**, and temperature is encoded in color. (B) Voltage-activated currents (top to bottom): wild-type, *gcy-8*, *gcy-18*, and *gcy-23* AFD neurons. Current evoked by a series of 100-ms voltage pulses applied between −110 and +110 mV (in 20-mV increments) from a holding potential of −60 mV. (C) Average peak (gray) and steady-state (black) current as a function of genotype (top to bottom): wild type, *gcy-8*, *gcy-18*, and *gcy-23*. At least seven recordings were obtained for each genotype, and error bars (SEM) were smaller than symbols in some cases. (D) Average ThRC amplitude, lifetime, and threshold *T** as a function of *gcy* genotype. For all parameters, only *gcy-8* was significantly different ($P < 0.05$) than wild type. Bars are the mean ± SEM of at least seven recordings for each genotype.

In particular, the increase in ThRC lifetime implies that PDEs normally act to restore cGMP to basal levels after a warming-evoked increase. To learn more about the likely PDE isoforms, we tested an inhibitor selective for mammalian PDE-2, BAY-60-7550, which also increased T^* and resulted in longer-lived ThRCs, a result that implies that AFD relies on a PDE-2–like enzyme for sensing temperature. Neither inhibitor had any detectable effect on the peak amplitude of warming-evoked ThRCs. These findings demonstrate that ThRC size is independent of PDE activity, but that this enzyme is essential for setting the threshold for CNG channel activation.

pde-2 and *pde-5* genes are expressed in AFD and required for thermotaxis

Next, we sought to identify which PDE genes are essential for AFD function, focusing on *pde-1*, *pde-2*, *pde-3*, and *pde-5*, which are predicted to hydrolyze cGMP and cAMP (Omori and Kotera, 2007). The remaining two *pde* genes, *pde-4* and *pde-6*, are predicted to be cAMP-selective enzymes (Omori and Kotera, 2007) and were not examined in this study. First, we screened *pde* mutants cultivated at 15°C for defects in migration on linear thermal gradients. When exposed to shallow thermal gradients (0.5°C/cm), *pde-1*, *pde-2*, *pde-3*, and *pde-5* mutants failed to sense the temperature changes properly and randomly distributed in the assay plate (Fig. 4 A). Interestingly, all four single mutants behaved like wild-type animals when exposed to steep gradients (1.5°C/cm) (Fig. 4 A). Thus, PDEs are necessary for proper thermotaxis and appear to be especially important for the ability to sense small temperature changes.

As with *gcy-8* mutants (Fig. 1 B), behavioral defects in *pde* mutants depended on cultivation temperature. For animals cultivated at 20°C, *pde-2*, *pde-3*, and *pde-5* mutant animals displayed normal thermotaxis responses under shallow gradients, whereas stronger defects were observed in the *pde-1* single mutants (Fig. 4 B). These data show that these four *pde* genes contribute to thermotaxis within specialized temperature ranges. To learn more about how *pde* genes regulate thermotaxis, we tested *pde-1–pde-2–pde-3–pde-5* quadruple mutants and found that these mutants displayed very strong defects in their response to both shallow (0.5°C/cm) and steep (1.5°C/cm) gradients (Fig. 4, A and B). Such behavioral defects were found in animals cultivated at both 15 and 20°C (Fig. 4, A and B). The severe defect in *pde* quadruple mutants and mild defects of single mutants suggest that these genes act in a partially redundant, degenerate manner.

Next, we asked whether any of the *pde* genes required for normal behavioral responses were expressed in the AFD neurons. To do this, we created transgenic animals coexpressing GFP under the control of the promoter of each *pde* gene and mCherry under the control of the AFD-specific promoter, *gcy-8*. As shown in Fig. 4 C, we found evidence that *pde-2* and *pde-5*, but not *pde-1* and *pde-3*, were expressed in AFD.

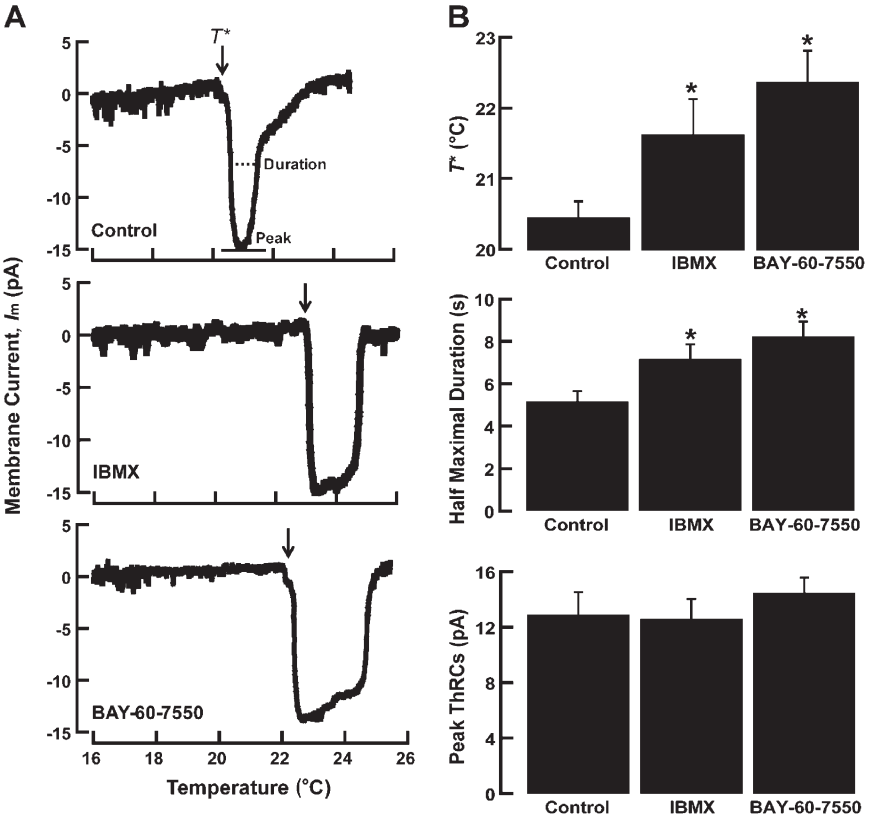

Figure 3. PDE inhibitors increase T^* and ThRC lifetime in wild-type ThRCs. (A) ThRCs in AFD neurons recorded with control intracellular saline (top) or with saline containing 200 µM IBMX (middle) or 1 µM BAY-60-7550 (bottom). Arrows indicate the T^* for ThRCs in each condition. $V_{hold} = -60$ mV and $T_{hold} = 20$°C. (B) Average T^*, half-maximal duration, and peak amplitude. Bars are the mean ± SEM of at least eight recordings in each condition. *, $P < 0.05$ compared with control.

Loss of PDE-2, but not of PDE-5, mimics the effect of PDE inhibition

To determine how *pde-2* and *pde-5* contribute to warming-evoked CNG channel activation in AFD neurons, we recorded ThRCs from AFD neurons in *pde-2* and *pde-5* mutant animals. As shown in Fig. 5 A, warming evokes a large inward current above T^* in wild-type, *pde-5*, and *pde-2* AFD neurons. We used Arrhenius plots of membrane current evoked by thermal ramps to quantify temperature sensitivity. As we have shown previously (Ramot et al., 2008a), such plots consisted of three domains (Fig. 5 B): a steep domain corresponding to activation of warming-evoked ThRCs flanked by two shallower ones. In agreement with previous work (Ramot et al., 2008a), apparent Q_{10} values for the steep domain varied between recordings but were >10^{15} in all cases. We could not detect any significant differences in apparent Q_{10} or activation energy as a function of *pde* genotype. Because loss of *pde-2* and *pde-5* had no detectable effect on Q_{10}, neither of these PDE proteins is likely to be rate-limiting for the nonlinear amplification process responsible for generating AFD ThRCs.

The value of T^* was similar in wild-type and *pde-5* mutant AFD recordings but was consistently higher in *pde-2* mutants (Fig. 5, B and C). ThRCs recorded in *pde-2* single mutants were indistinguishable from those recorded in *pde-2–pde-5* double mutants (Fig. 5 C), implying that *pde-2*, but not *pde-5*, is essential to regulate T^*. Interestingly, although the peak amplitude of the ThRCs was not affected by loss of *pde-2* function, the lifetime of the warming-activated ThRC was significantly increased in *pde-2* mutants compared with wild type (Fig. 5, A–C). Thus, as in wild-type neurons treated with IBMX and PDE2-selective inhibitors, loss of PDE activity increases

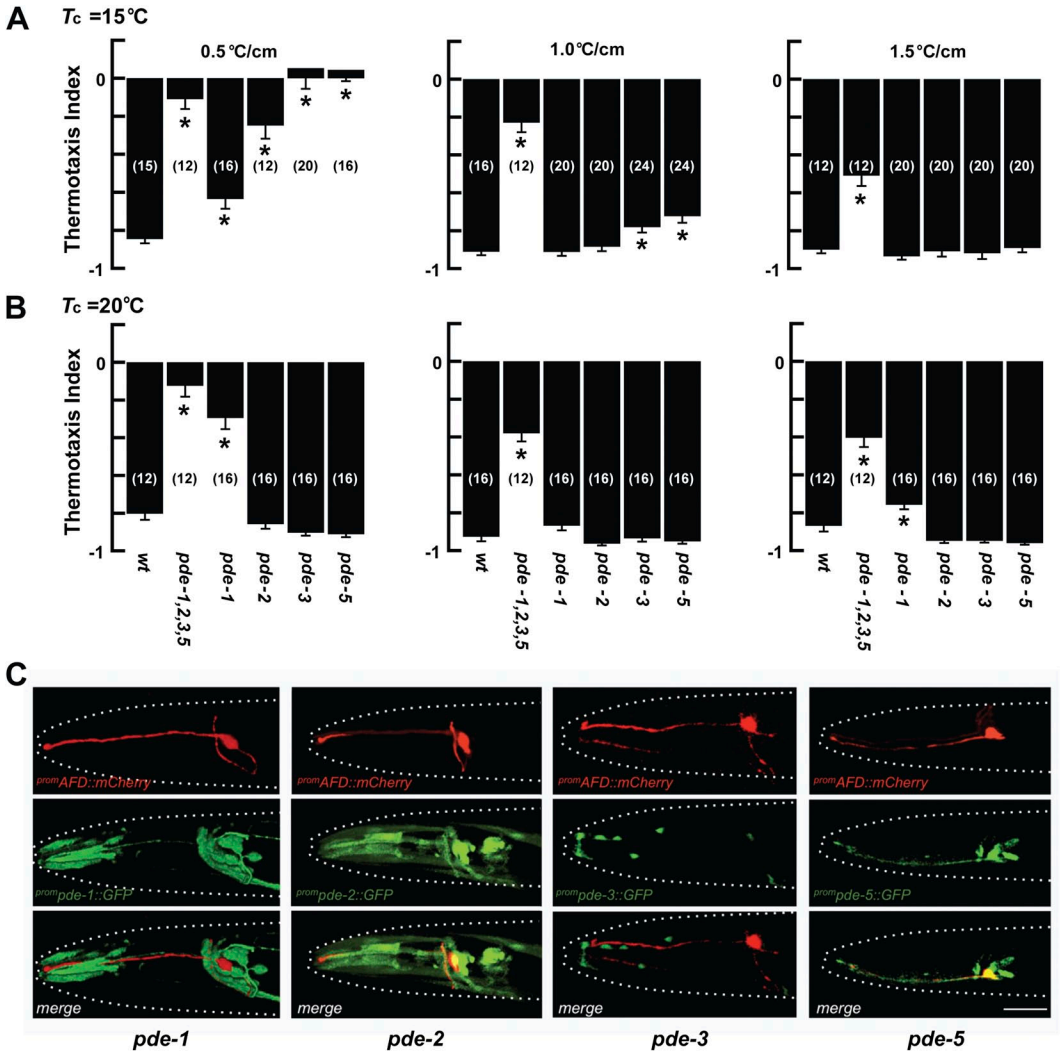

Figure 4. Thermotaxis depends on at least four *pde* genes, of which two are expressed in AFD. (A and B) Thermotaxis response profiles of *pde* mutants at T_c = 15°C and T_c = 20°C. Bars are mean ± SEM; the number of assays is indicated in parentheses. *, P < 0.05 compared with wild type. (C) Fluorescent micrographs of double transgenic lines coexpressing mCherry in AFD and GFP under the control of promoters for each *pde* gene. Top row, ^{prom}AFD::mCherry in the AFD neuron; middle row, GFP reporters for the *pde-1*, *pde-2*, *pde-3*, or *pde-5* genes; bottom row, merged image. Bar, 10 µm.

T^* and the ThRC lifetime. We could not detect an effect of loss of PDE activity on rise time with pharmacological nor genetic inhibition of PDE activity. Voltage-activated currents in wild-type and *pde-2* mutant AFD neurons are similar, suggesting that the mutation in *pde-2* selectively affects warming-activated currents in AFD neurons (Fig. 5 D). Collectively, our results indicate that reducing PDE function either pharmacologically or genetically increases T^* as well as the lifetime of warming-activated ThRCs. From these findings, we infer that warming normally inhibits PDE activity to increase intracellular cGMP concentration, activate CNG channels, and fine-tune T^*.

PDE-2 regulates the relationship between T^* and T_{hold}

Previous work has shown that T^* is independent of cultivation temperature (T_c) but depends on the holding temperature (T_{hold}) of the bath solution during the recording (Ramot et al., 2008a). Above, we established that decreasing PDE activity through pharmacological inhibition or genetic deletion increases T^* relative to wild type. All of these data were collected from well-fed animals cultivated at 20°C and for holding temperatures of 20°C. Next, we asked how loss of *pde-2* affected the relationship between T^* and T_{hold}. In contrast with wild-type AFD neurons, the application of a holding temperature of 17°C for at least 15 min to *pde-2* mutant AFD neurons failed to shift T^* to the new temperature (Fig. 6, A and B). This finding implies that PDE-2 is required for the dynamic adaptation of T^*. Consistent with misregulation of temperature-dependent cGMP dynamics, the duration of the response was extended in *pde-2* mutants compared with wild type across a range of

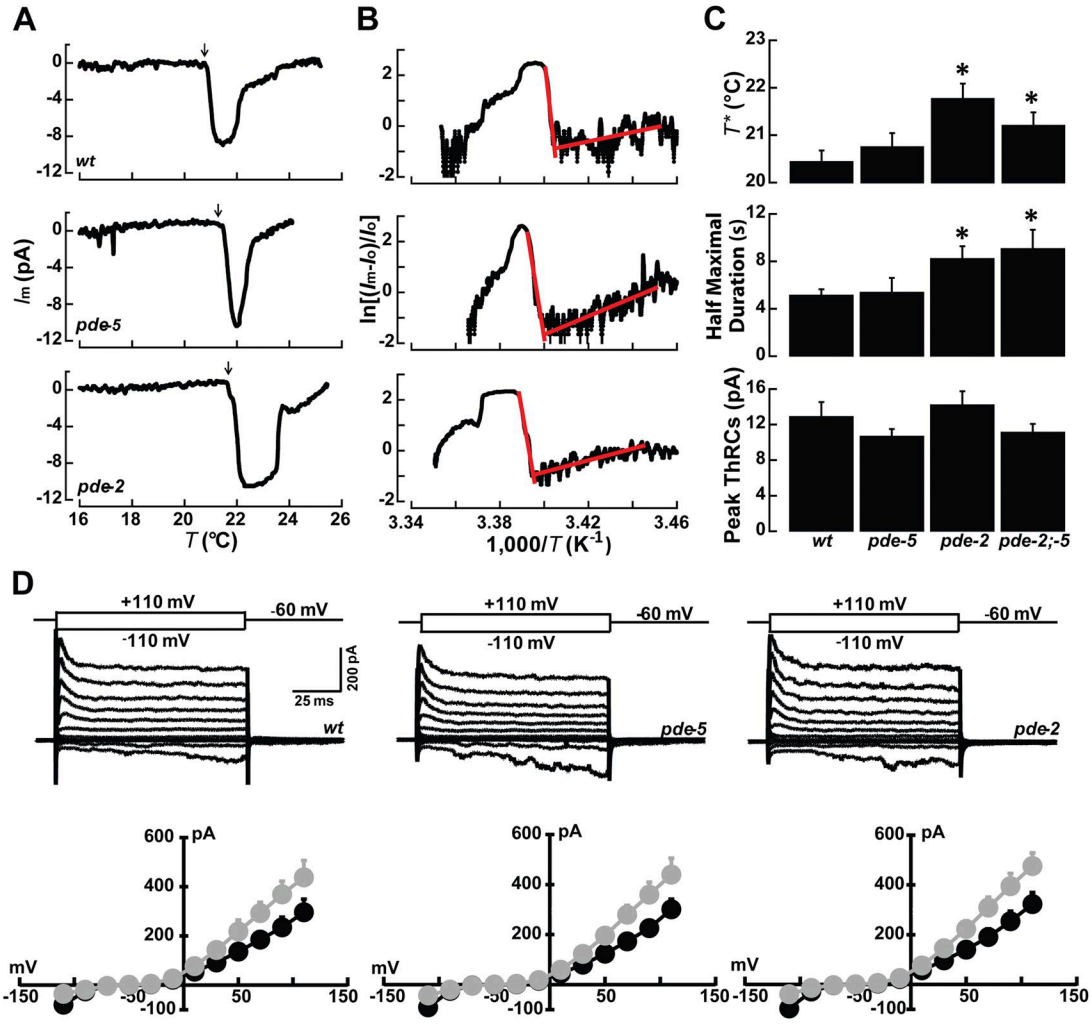

Figure 5. Deleting *pde-2* elevates T^* and prolongs ThRC lifetime but has no effect on voltage-activated currents. (A) ThRCs in wild-type (top), *pde-5* (middle), and *pde-2* mutant (bottom) AFD neurons. Arrows indicate T^*. $V_{hold} = -60$ mV. (B) Arrhenius plots of warming-activated currents from the same recordings as in A. Red line indicates the linear fit to the two phases of the normalized ThRCs. Apparent Q_{10} was calculated from the slope of the linear fit. (C) Average T^*, half-maximal duration, and peak amplitude. Bars are the mean ± SEM of at least eight recordings in each genotype. *, $P < 0.05$ compared with wild type. (D; top) Voltage-activated currents in wild-type (left), *pde-5* (middle), and *pde-2* (right) AFD neurons. Traces are the average of the response to three presentations of a series of voltage pulses between −110 and +110 mV in 20-mV increments from a holding potential of −60 mV. (Bottom) Peak (gray) and steady-state (black) I-V relationship in wild-type (left), *pde-5* (middle), and *pde-2* (right) AFD neurons ($n \geq 8$). $V_{hold} = -60$ mV.

holding temperatures (Fig. 6 C). However, holding temperature had little, if any, effect on ThRC amplitude (Fig. 6 D), suggesting that this parameter is independent of PDE activity and likely to be set by the maximum number of CNG channels available for activation.

NCS-1 regulates T^*

NCS-1 belongs to a family of calcium sensor proteins that play multiple roles in neurons and includes the GCAPs (Burgoyne, 2007; Burgoyne and Haynes, 2012). In vertebrate photoreceptors, GCAPs provide calcium-dependent negative feedback to regulate cGMP synthesis (Schaad et al., 1996; Mendez et al., 2001). Given that *ncs-1* is expressed in the AFD neurons and regulates behavioral responses to thermal gradients (Gomez et al., 2001), we hypothesized that NCS-1 protein might also help to fine-tune ThRCs. We tested this idea by recording ThRCs in *ncs-1* mutant AFD neurons and found that loss of *ncs-1* function increased T^* by 4°C (wild-type T^*: 20.4 ± 0.2°C; *ncs-1* T^*: 24.4 ± 0.3°C) and significantly increased ThRC lifetime (Fig. 7, A and B). Thus, NCS-1 and PDE-2 have similar functional roles in AFD thermotransduction. In contrast with *gcy-8* and *pde-2* mutations, which affect ThRCs but not voltage-gated currents, loss of function *ncs-1* increased voltage-activated outward currents (Fig. 7, C and D). This result suggests that NCS-1 inhibits one or more voltage-gated K^+ channels in the AFD neurons. Similar results have been reported in Purkinje neurons (Xia et al., 2010). Thus, NCS-1 regulates the activation of at least two classes of ion channels in the AFD neurons: the TAX-4/2–dependent CNG channel and a voltage-gated K^+ channel whose identity is not yet known.

DISCUSSION

Many sensory transduction cascades, including those responsible for vertebrate vision and olfaction, regulate the concentration of cyclic nucleotides inside sensory endings and result in electrical signals by regulating the activity of CNG ion channels localized to specialized sensory cilia (Kleene, 2008; Fain et al., 2010; Kaupp, 2010; Yildiz and Khanna, 2012). From the present experiments, we draw two main conclusions about AFD thermotransduction: PDE activity helps to set both the threshold, T^*, and the lifetime of ThRCs, and, of two PDE genes expressed in AFD, only PDE-2 is required for responses to temperature. Because work extending over the past decade has shown that AFD function depends on a signaling network that includes guanylate cyclases and a cGMP-gated ion channel (Kimura et al., 2004; Clark et al., 2006; Ramot et al., 2008a; Wasserman et al.,

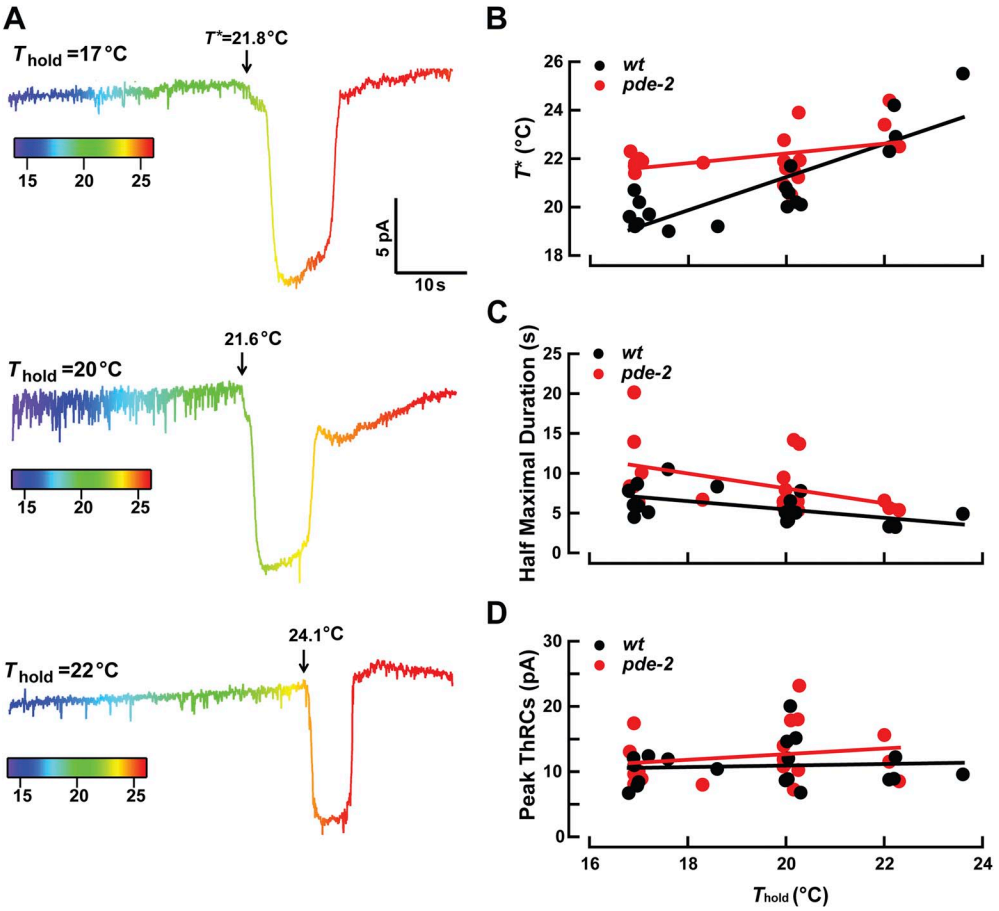

Figure 6. PDE-2 is required for ThRC adaptation. (A) ThRCs recorded in *pde-2* mutant AFDs from a holding temperature of 17°C (top), 20°C (middle), or 22°C (bottom). V_{hold} = −60 mV. Arrows indicate T^*. (B) Threshold for ThRC activation, T^*, versus T_{hold} in wild-type (*wt*; black) and *pde-2* (red) mutant AFD neurons. Lines are a linear fit to the data, showing a stronger correlation between T^* and T_{hold} for wild type (R^2 = 0.69) compared with *pde-2* (R^2 = 0.15). All animals were cultivated at 20°C. (C) Half-maximal duration plot versus T_{hold} from AFD neurons in wild-type and *pde-2* mutants. R^2 = 0.31 for the linear fit from wild-type and R^2 = 0.19 from *pde-2* mutants. (D) Peak amplitude of ThRCs versus T_{hold} for AFD neurons in wild-type and *pde-2* mutants. R^2 = 0.006 for the linear fit from wild-type and R^2 = 0.04 from *pde-2* mutants.

2011), it is not surprising that PDE activity contributes to AFD thermotransduction. The utility of the present experiments is that they directly show that PDE activity is required for AFD thermotransduction and that T^*, but not the size or apparent Q_{10} of warming-evoked ThRCs, depends on full PDE activity. They also identify PDE-2 as a key regulator of thermotransduction. Our results have implications for understanding the molecular events that give rise to ThRCs in AFD, especially their adaptable threshold for initiation, T^*, and also for cGMP-dependent signaling more generally.

Coordinated cGMP synthesis and hydrolysis underlies AFD thermotransduction

The AFD neurons can detect minute fluctuations in temperature, and this ability is known to depend on GCY-8, GCY-18, and GCY-23, three AFD-specific GCY proteins predicted to catalyze cGMP synthesis, and on cGMP-activated TAX-4/2 channels (Coburn and Bargmann, 1996; Komatsu et al., 1996; Inada et al., 2006; Ramot et al., 2008a). Consistent with prior work showing that most *gcy-8* mutant AFD neurons fail to generate calcium signals in response to thermal fluctuations (Wasserman et al., 2011), the present experiments show that GCY-8 is critical for the generation of full amplitude ThRCs in AFD neurons studied (Fig. 2). We also establish that *pde-2*, a gene encoding a putative PDE expected to catalyze the conversion of cGMP into its linear monophosphate form, regulates the threshold for ThRC activation as well as its lifetime. Thus, PDE activity fine-tunes ThRC properties, but PDE-2 is unlikely to be the sole arbiter of temperature-dependent modulation of intracellular cGMP. Indeed, at least two aspects of ThRC activation are unaffected by defects in the *pde-2* gene or by inhibition of PDE activity. For instance, ThRC amplitude is not affected by genetic or pharmacological inhibition of PDE activity (Figs. 3 and 5 C), a finding that suggests this inference: the number of channels available for activation defines ThRC amplitude but not the level of intracellular cGMP achieved during warming. Additionally, apparent Q_{10} values were indistinguishable in recordings from wild-type and *pde-2* mutant AFD neurons (Fig. 5 B). Thus, the extraordinary sensitivity of AFD neurons to temperature change may be dominated by temperature-dependent modulation of cGMP synthesis, whereas hydrolysis is crucial for adaptation.

The relationship between cGMP and T^*

Loss of PDE activity through small-molecule inhibition (Fig. 3 B) or genetic deletion (Fig. 5 C) elevates T^*. If such manipulations increase intracellular cGMP as expected, treating wild-type animals with a nonhydrolyzable analogue of cGMP such as 8-Br-cGMP should also increase T^*. Although we could not detect any effect of including 8-Br-cGMP in the recording pipette on the generation of ThRCs (not depicted), exogenous 8-bromo-cGMP does increase T^* for warming-evoked calcium transients (Wasserman et al., 2011). But we note that even in wild-type AFD neurons, the value for T^* is not fixed. Rather, T^* is strongly coupled to holding temperature under control conditions (Fig. 6, A and B, and Ramot et al., 2008a). This relationship reflects an adaptation process that adjusts T^* relative to recent thermal history at a rate that depends on intracellular calcium buffering (Ramot et al., 2008a). The coupling between holding temperature and T^* is profoundly reduced in *pde-2* mutants (Fig. 6 B), indicating that PDE-2 is required for proper adaptation of T^* and underscoring

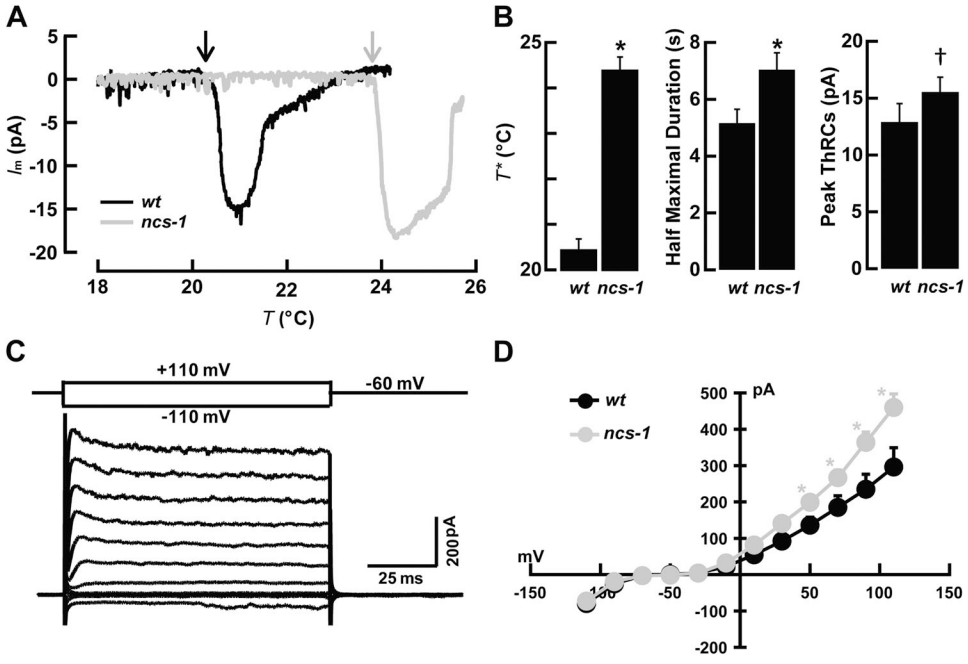

Figure 7. NCS-1 regulates ThRCs and voltage-activated currents in AFD neurons. (A) ThRCs in wild-type (*wt*; black) and *ncs-1* (red) mutant AFD neurons. V_{hold} = −60 mV. Arrows indicate T^*. (B) Average T^*, half-maximal duration, and peak amplitude of ThRCs in wild-type (n = 8) and *ncs-1* mutants (n = 10). *, P < 0.05 compared with wild type; †, not significantly different from wild type. (C) Voltage-activated currents in *ncs-1* mutant AFD neurons. Traces are the average of the response to three presentations of a series of voltage pulses between −110 and +110 mV in 20-mV increments from a holding potential of −60 mV. (D) Steady-state I-V relationship in wild-type (n = 8) and *ncs-1* mutants (n = 10). *, P < 0.05 compared with wild type.

the idea that loss of PDE-2 has a complex impact on cGMP signaling in AFD.

Deleting NCS-1 also elevates T^* without affecting either the holding current or ThRC amplitude (Fig. 7, A and B). Frequenin, the human homologue of the *C. elegans* NCS-1 protein (Shaye and Greenwald, 2011), potentiates PDE activity in a calcium-dependent manner in vitro (Schaad et al., 1996). Thus, if *C. elegans* NCS-1 functions like its human counterpart, it is no surprise that loss of NCS-1 and PDE-2 produces similar effects on T^*, holding current, and ThRC amplitude. However, *ncs-1* mutant AFD neurons held at 20°C had much higher values than *pde-2* mutants for T^* (21.8 ± 0.3°C vs. 24.4 ± 0.3°C), a result that suggests that NCS-1 could modulate the activity of additional targets. NCS-1 is also related to the GCAPs that mediate calcium-dependent feedback of guanylate cyclase activity in rod photoreceptors (Mendez et al., 2001). On this basis, we propose that NCS-1 also serves this function in the AFD neurons. Thus, NCS-1 could regulate cGMP synthesis in AFD neurons by increasing PDE activity and by decreasing GCY activity in a calcium-dependent manner. This scenario is consistent with our observation that deleting NCS-1 significantly increases ThRC lifetime (Fig. 7, A and B).

Thus, manipulations predicted to increase intracellular cGMP (PDE inhibitors or *pde-2* and *ncs-1* mutants) elevate T^*. The mechanism responsible for this change in sensory thermotransduction remains unclear. Two possibilities that are consistent with the existing data are: (1) a cGMP-dependent decrease in the sensitivity of the TAX-4/2 channel for its ligand; or (2) a homeostatic, cGMP-dependent decrease in GCY activity (Kuwayama and Van Haastert, 1996; Ferrero et al., 2000; Murthy, 2004). We favor the second model, illustrated in Fig. 8, which could act to reestablish the balance between cGMP synthesis and hydrolysis under resting conditions after perturbation of cGMP concentration, while also elevating T^*. Additional work will be needed to test this model in depth.

NCS-1 has a dual function in AFD

In contrast with other genes needed for normal ThRCs (this study and Ramot et al., 2008a), loss of *ncs-1* function alters both ThRCs recorded at constant voltage and voltage-activated currents recorded at constant temperature (20°C). In particular, we find that voltage-activated outward currents are increased in *ncs-1* mutants compared with wild type (Fig. 7 D). This finding suggests that *ncs-1* is a negative regulator of a voltage-activated K^+ channel in AFD, and that loss of *ncs-1* could inhibit AFD signaling by increasing the activity of K^+ channels that normally oppose depolarization. Precedent for this idea comes from KChIP proteins, which share significant sequence homology with NCS-1 frequenin and are known to regulate mammalian K^+ channels (Xia et al., 2010). Although the molecular identity of the K^+ channel target of NCS-1 in AFD is not yet known, the dual effect of NCS-1 on ThRCs and voltage-activated currents suggests that *ncs-1* mutants have severe defects in AFD signaling.

Thermotransduction in AFD

We propose that temperature regulates the activity of both GCY-8 and PDE-2 to achieve a sharp but adjustable threshold, T^*, for CNG channel activation and that both enzymes are subject to NCS-1–mediated feedback control (Fig. 8). Significant open questions remain, including the understanding of whether or not temperature regulates cGMP synthesis and hydrolysis by acting on GCY-8 and PDE-2 directly. In support of the idea that GCY activity could be directly modulated by temperature, the synthetic activity of another *C. elegans* guanylate cyclase, GCY-12, has a bell-shaped dependence on temperature when expressed in heterologous cells (Baude

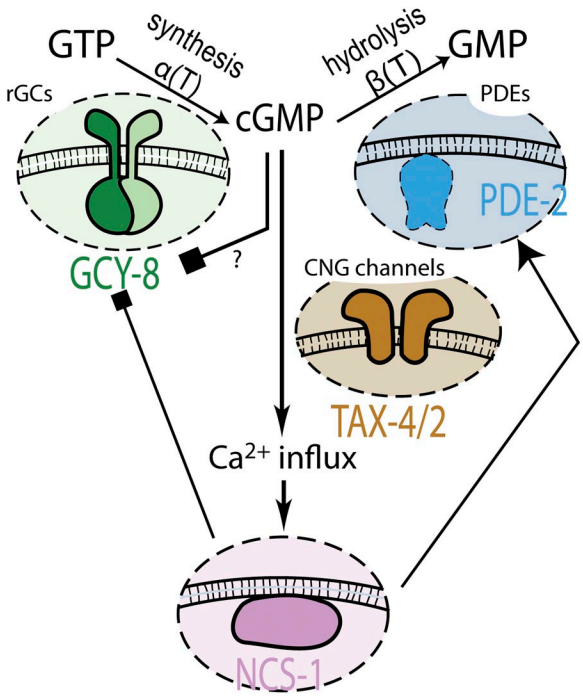

Figure 8. Molecular model for thermotransduction in AFD. Diagram of the proposed interplay of cGMP production, CNG channel activation, and calcium influx in AFD neurons. In this model, intracellular cGMP concentration depends on the activities of rGCs, which synthesize cGMP and PDEs, which degrade cGMP. Calcium influx through the CNG channel further regulates NCS-1, which may provide negative feedback on cGMP production by inhibiting GCYs or potentiating PDE. Because manipulations expected to increase cGMP do not increase holding current, we propose a homeostatic mechanism whereby cGMP down-regulates GCY activity through an unknown cGMP-binding protein. Bubbles show the proteins linked in this study and in Ramot et al. (2008a) to the generation and adaptation of warming-evoked ThRCs. It is not known if the putative temperature dependence of cGMP synthesis and hydrolysis is conferred by an upstream receptor or is an intrinsic property of one or both enzymes.

et al., 1997; Yu et al., 1997). The picture emerging from genetic dissection of ThRCs in AFD is that temperature acts on both GCY and PDE proteins to regulate the concentration of cGMP, and that NCS-1 mediates calcium-dependent negative feedback on cGMP synthesis in this network.

We thank S. Lasse and S. Katta for comments; E. Martinez-Nieves for help with initial *pde* experiments; S. Mitani, I. Mori, P. Sengupta, S. Xu, the *C. elegans* Knockout Consortium, and the Caenorhabditis Genetics Center, which is funded by the National Institutes of Health (NIH) National Center for Research Resources, for strains.

This work is supported by grants from NIH (R21 NS061147) and the National Science Foundation (IOS 0725079) to M.B. Goodman and a Dean's Fellowship from Stanford University School of Medicine to D. Wang.

Sharona E. Gordon served as editor.

Submitted: 7 January 2013
Accepted: 30 August 2013

REFERENCES

Arshavsky, V.Y., and M.E. Burns. 2012. Photoreceptor signaling: supporting vision across a wide range of light intensities. *J. Biol. Chem.* 287:1620–1626. http://dx.doi.org/10.1074/jbc.R111.305243

Baude, E.J., V.K. Arora, S. Yu, D.L. Garbers, and B.J. Wedel. 1997. The cloning of a *Caenorhabditis elegans* guanylyl cyclase and the construction of a ligand-sensitive mammalian/nematode chimeric receptor. *J. Biol. Chem.* 272:16035–16039. http://dx.doi.org/10.1074/jbc.272.25.16035

Beverly, M., S. Anbil, and P. Sengupta. 2011. Degeneracy and neuromodulation among thermosensory neurons contribute to robust thermosensory behaviors in *Caenorhabditis elegans*. *J. Neurosci.* 31:11718–11727.http://dx.doi.org/10.1523/JNEUROSCI.1098-11.2011

Biron, D., M. Shibuya, C. Gabel, S.M. Wasserman, D.A. Clark, A. Brown, P. Sengupta, and A.D. Samuel. 2006. A diacylglycerol kinase modulates long-term thermotactic behavioral plasticity in *C. elegans*. *Nat. Neurosci.* 9:1499–1505. http://dx.doi.org/10.1038/nn1796

Biron, D., S. Wasserman, J.H. Thomas, A.D. Samuel, and P. Sengupta. 2008. An olfactory neuron responds stochastically to temperature and modulates *Caenorhabditis elegans* thermotactic behavior. *Proc. Natl. Acad. Sci. USA.* 105:11002–11007. http://dx.doi.org/10.1073/pnas.0805004105

Bullock, T.H., and F.P. Diecke. 1956. Properties of an infra-red receptor. *J. Physiol.* 134:47–87.

Burgoyne, R.D. 2007. Neuronal calcium sensor proteins: generating diversity in neuronal Ca^{2+} signalling. *Nat. Rev. Neurosci.* 8:182–193. http://dx.doi.org/10.1038/nrn2093

Burgoyne, R.D., and L.P. Haynes. 2012. Understanding the physiological roles of the neuronal calcium sensor proteins. *Mol. Brain.* 5:2. http://dx.doi.org/10.1186/1756-6606-5-2

Campbell, A.L., R.R. Naik, L. Sowards, and M.O. Stone. 2002. Biological infrared imaging and sensing. *Micron.* 33:211–225. http://dx.doi.org/10.1016/S0968-4328(01)00010-5

Chi, C.A., D.A. Clark, S. Lee, D. Biron, L. Luo, C.V. Gabel, J. Brown, P. Sengupta, and A.D. Samuel. 2007. Temperature and food mediate long-term thermotactic behavioral plasticity by association-independent mechanisms in *C. elegans*. *J. Exp. Biol.* 210:4043–4052. http://dx.doi.org/10.1242/jeb.006551

Clark, D.A., D. Biron, P. Sengupta, and A.D. Samuel. 2006. The AFD sensory neurons encode multiple functions underlying thermotactic behavior in *Caenorhabditis elegans*. *J. Neurosci.* 26:7444–7451. http://dx.doi.org/10.1523/JNEUROSCI.1137-06.2006

Coburn, C.M., and C.I. Bargmann. 1996. A putative cyclic nucleotide-gated channel is required for sensory development and function in *C. elegans*. *Neuron.* 17:695–706. http://dx.doi.org/10.1016/S0896-6273(00)80201-9

Fain, G.L., R. Hardie, and S.B. Laughlin. 2010. Phototransduction and the evolution of photoreceptors. *Curr. Biol.* 20:R114–R124. http://dx.doi.org/10.1016/j.cub.2009.12.006

Fay, D. 2006. Genetic mapping and manipulation: chapter 1—Introduction and basics. *WormBook.* 17:1–12.

Ferrero, R., F. Rodríguez-Pascual, M.T. Miras-Portugal, and M. Torres. 2000. Nitric oxide-sensitive guanylyl cyclase activity inhibition through cyclic GMP-dependent dephosphorylation. *J. Neurochem.* 75:2029–2039. http://dx.doi.org/10.1046/j.1471-4159.2000.0752029.x

Fu, Y., and K.W. Yau. 2007. Phototransduction in mouse rods and cones. *Pflugers Arch.* 454:805–819. http://dx.doi.org/10.1007/s00424-006-0194-y

Garrity, P.A., M.B. Goodman, A.D. Samuel, and P. Sengupta. 2010. Running hot and cold: behavioral strategies, neural circuits, and the molecular machinery for thermotaxis in *C. elegans* and *Drosophila*. *Genes Dev.* 24:2365–2382. http://dx.doi.org/10.1101/gad.1953710

Glauser, D.A., W.C. Chen, R. Agin, B.L. Macinnis, A.B. Hellman, P.A. Garrity, M.W. Tan, and M.B. Goodman. 2011. Heat avoidance is regulated by transient receptor potential (TRP) channels and a neuropeptide signaling pathway in *Caenorhabditis elegans*. *Genetics.* 188:91–103. http://dx.doi.org/10.1534/genetics.111.127100

Gomez, M., E. De Castro, E. Guarin, H. Sasakura, A. Kuhara, I. Mori, T. Bartfai, C.I. Bargmann, and P. Nef. 2001. Ca^{2+} signaling via the neuronal calcium sensor-1 regulates associative learning and memory in *C. elegans*. *Neuron.* 30:241–248. http://dx.doi.org/10.1016/S0896-6273(01)00276-8

Goodman, M.B., and S.R. Lockery. 2000. Pressure polishing: a method for re-shaping patch pipettes during fire polishing. *J. Neurosci. Methods.* 100:13–15. http://dx.doi.org/10.1016/S0165-0270(00)00224-7

Goodman, M.B., D.H. Hall, L. Avery, and S.R. Lockery. 1998. Active currents regulate sensitivity and dynamic range in *C. elegans* neurons. *Neuron.* 20:763–772. http://dx.doi.org/10.1016/S0896-6273(00)81014-4

Goodman, M.B., T.H. Lindsay, S.R. Lockery, and J.E. Richmond. 2012. Electrophysiological methods for *Caenorhabditis elegans* neurobiology. *Methods Cell Biol.* 107:409–436. http://dx.doi.org/10.1016/B978-0-12-394620-1.00014-X

Gracheva, E.O., N.T. Ingolia, Y.M. Kelly, J.F. Cordero-Morales, G. Hollopeter, A.T. Chesler, E.E. Sánchez, J.C. Perez, J.S. Weissman, and D. Julius. 2010. Molecular basis of infrared detection by snakes. *Nature.* 464:1006–1011. http://dx.doi.org/10.1038/nature08943

Gracheva, E.O., J.F. Cordero-Morales, J.A. González-Carcacía, N.T. Ingolia, C. Manno, C.I. Aranguren, J.S. Weissman, and D. Julius. 2011. Ganglion-specific splicing of TRPV1 underlies infrared sensation in vampire bats. *Nature.* 476:88–91. http://dx.doi.org/10.1038/nature10245

Hahm, J.H., S. Kim, and Y.K. Paik. 2009. Endogenous cGMP regulates adult longevity via the insulin signaling pathway in *Caenorhabditis elegans*. *Aging Cell.* 8:473–483. http://dx.doi.org/10.1111/j.1474-9726.2009.00495.x

Hedgecock, E.M., and R.L. Russell. 1975. Normal and mutant thermotaxis in the nematode *Caenorhabditis elegans*. *Proc. Natl. Acad. Sci. USA.* 72:4061–4065. http://dx.doi.org/10.1073/pnas.72.10.4061

Hobert, O. 2002. PCR fusion-based approach to create reporter gene constructs for expression analysis in transgenic *C. elegans*. *Biotechniques*. 32:728–730.

Inada, H., H. Ito, J. Satterlee, P. Sengupta, K. Matsumoto, and I. Mori. 2006. Identification of guanylyl cyclases that function in thermosensory neurons of *Caenorhabditis elegans*. *Genetics*. 172: 2239–2252. http://dx.doi.org/10.1534/genetics.105.050013

Johnson, B.E., A.L. Brown, and M.B. Goodman. 2008. Pressure-polishing pipettes for improved patch-clamp recording. *J. Vis. Exp*. 20:964.

Kaupp, U.B. 2010. Olfactory signalling in vertebrates and insects: differences and commonalities. *Nat. Rev. Neurosci*. 11:188–200.

Kimura, K.D., A. Miyawaki, K. Matsumoto, and I. Mori. 2004. The *C. elegans* thermosensory neuron AFD responds to warming. *Curr. Biol*. 14:1291–1295. http://dx.doi.org/10.1016/j.cub.2004.06.060

Kleene, S.J. 2008. The electrochemical basis of odor transduction in vertebrate olfactory cilia. *Chem. Senses*. 33:839–859. http://dx.doi.org/10.1093/chemse/bjn048

Komatsu, H., I. Mori, J.S. Rhee, N. Akaike, and Y. Ohshima. 1996. Mutations in a cyclic nucleotide-gated channel lead to abnormal thermosensation and chemosensation in *C. elegans*. *Neuron*. 17:707–718. http://dx.doi.org/10.1016/S0896-6273(00)80202-0

Kuhara, A., M. Okumura, T. Kimata, Y. Tanizawa, R. Takano, K.D. Kimura, H. Inada, K. Matsumoto, and I. Mori. 2008. Temperature sensing by an olfactory neuron in a circuit controlling behavior of *C. elegans*. *Science*. 320:803–807. http://dx.doi.org/10.1126/science.1148922

Kuwayama, H., and P.J. Van Haastert. 1996. Regulation of guanylyl cyclase by a cGMP-binding protein during chemotaxis in *Dictyostelium discoideum*. *J. Biol. Chem*. 271:23718–23724. http://dx.doi.org/10.1074/jbc.271.39.23718

Liu, J., A. Ward, J. Gao, Y. Dong, N. Nishio, H. Inada, L. Kang, Y. Yu, D. Ma, T. Xu, et al. 2010. *C. elegans* phototransduction requires a G protein-dependent cGMP pathway and a taste receptor homolog. *Nat. Neurosci*. 13:715–722. http://dx.doi.org/10.1038/nn.2540

Luo, L., D.A. Clark, D. Biron, L. Mahadevan, and A.D. Samuel. 2006. Sensorimotor control during isothermal tracking in *Caenorhabditis elegans*. *J. Exp. Biol*. 209:4652–4662. http://dx.doi.org/10.1242/jeb.02590

Mendez, A., M.E. Burns, I. Sokal, A.M. Dizhoor, W. Baehr, K. Palczewski, D.A. Baylor, and J. Chen. 2001. Role of guanylate cyclase-activating proteins (GCAPs) in setting the flash sensitivity of rod photoreceptors. *Proc. Natl. Acad. Sci. USA*. 98:9948–9953. http://dx.doi.org/10.1073/pnas.171308998

Mori, I. 1999. Genetics of chemotaxis and thermotaxis in the nematode *Caenorhabditis elegans*. *Annu. Rev. Genet*. 33:399–422. http://dx.doi.org/10.1146/annurev.genet.33.1.399

Mori, I., and Y. Ohshima. 1995. Neural regulation of thermotaxis in *Caenorhabditis elegans*. *Nature*. 376:344–348. http://dx.doi.org/10.1038/376344a0

Murthy, K.S. 2004. Modulation of soluble guanylate cyclase activity by phosphorylation. *Neurochem. Int*. 45:845–851. http://dx.doi.org/10.1016/j.neuint.2004.03.014

Must, A., E. Merivee, A. Luik, I. Williams, A. Ploomi, and M. Heidemaa. 2010. Spike bursts generated by the thermosensitive (cold) neuron from the antennal campaniform sensilla of the ground beetle *Platynus assimilis*. *J. Insect Physiol*. 56:412–421. http://dx.doi.org/10.1016/j.jinsphys.2009.11.017

Omori, K., and J. Kotera. 2007. Overview of PDEs and their regulation. *Circ. Res*. 100:309–327. http://dx.doi.org/10.1161/01.RES.0000256354.95791.f1

Ramot, D., B.L. MacInnis, and M.B. Goodman. 2008a. Bidirectional temperature-sensing by a single thermosensory neuron in *C. elegans*. *Nat. Neurosci*. 11:908–915. http://dx.doi.org/10.1038/nn.2157

Ramot, D., B.L. MacInnis, H.C. Lee, and M.B. Goodman. 2008b. Thermotaxis is a robust mechanism for thermoregulation in *Caenorhabditis elegans* nematodes. *J. Neurosci*. 28:12546–12557. http://dx.doi.org/10.1523/JNEUROSCI.2857-08.2008

Ryu, W.S., and A.D. Samuel. 2002. Thermotaxis in *Caenorhabditis elegans* analyzed by measuring responses to defined thermal stimuli. *J. Neurosci*. 22:5727–5733.

Schaad, N.C., E. De Castro, S. Nef, S. Hegi, R. Hinrichsen, M.E. Martone, M.H. Ellisman, R. Sikkink, F. Rusnak, J. Sygush, and P. Nef. 1996. Direct modulation of calmodulin targets by the neuronal calcium sensor NCS-1. *Proc. Natl. Acad. Sci. USA*. 93:9253–9258. http://dx.doi.org/10.1073/pnas.93.17.9253

Schmitz, H., and S. Trenner. 2003. Electrophysiological characterization of the multipolar thermoreceptors in the "fire-beetle" *Merimna atrata* and comparison with the infrared sensilla of *Melanophila acuminata* (both Coleoptera, Buprestidae). *J. Comp. Physiol. A Neuroethol. Sens. Neural Behav. Physiol*. 189:715–722. http://dx.doi.org/10.1007/s00359-003-0447-6

Shaye, D.D., and I. Greenwald. 2011. OrthoList: a compendium of *C. elegans* genes with human orthologs. *PLoS ONE*. 6:e20085. http://dx.doi.org/10.1371/journal.pone.0020085

Ward, S., N. Thomson, J.G. White, and S. Brenner. 1975. Electron microscopical reconstruction of the anterior sensory anatomy of the nematode *Caenorhabditis elegans*. *J. Comp. Neurol*. 160:313–337. http://dx.doi.org/10.1002/cne.901600305

Wasserman, S.M., M. Beverly, H.W. Bell, and P. Sengupta. 2011. Regulation of response properties and operating range of the AFD thermosensory neurons by cGMP signaling. *Curr. Biol*. 21:353–362. http://dx.doi.org/10.1016/j.cub.2011.01.053

White, J.G., E. Southgate, J.N. Thomson, and S. Brenner. 1986. The structure of the nervous system of the nematode *Caenorhabditis elegans*. *Philos. Trans. R. Soc. Lond. B Biol. Sci*. 314:1–340. http://dx.doi.org/10.1098/rstb.1986.0056

Xia, K., H. Xiong, Y. Shin, D. Wang, T. Deerinck, H. Takahashi, M.H. Ellisman, S.A. Lipton, G. Tong, G. Descalzi, et al. 2010. Roles of KChIP1 in the regulation of GABA-mediated transmission and behavioral anxiety. *Mol. Brain*. 3:23. http://dx.doi.org/10.1186/1756-6606-3-23

Yildiz, O., and H. Khanna. 2012. Ciliary signaling cascades in photoreceptors. *Vision Res*. 75:112–116. http://dx.doi.org/10.1016/j.visres.2012.08.007

Yu, S., L. Avery, E. Baude, and D.L. Garbers. 1997. Guanylyl cyclase expression in specific sensory neurons: a new family of chemosensory receptors. *Proc. Natl. Acad. Sci. USA*. 94:3384–3387. http://dx.doi.org/10.1073/pnas.94.7.3384